ELSEVIER

Contents lists available at ScienceDirect

Journal of Computational and Applied Mathematics

journal homepage: www.elsevier.com/locate/cam



A primal-dual finite element method for transport equations in non-divergence form



Dan Li^a, Chunmei Wang^{b,*,1}, Junping Wang^{c,2}

- ^a Department of Applied Mathematics, Northwestern Polytechnical University, Xi'an, Shannxi 710072, China
- ^b Department of Mathematics, University of Florida, Gainesville, FL 32611, United States of America
- ^c Division of Mathematical Sciences, National Science Foundation, Alexandria, VA 22314, United States of America

ARTICLE INFO

Article history:

Received 12 September 2020 Received in revised form 6 February 2022

MSC: Primary 65N30 65N15 65N12 Secondary 35L02

35F15

Keywords: Primal-dual weak Galerkin Finite element method Weak Galerkin

Discrete weak gradient

Transport equation Non-divergence

ABSTRACT

This article presents a new primal-dual weak Galerkin (PDWG) finite element method for transport equations in non-divergence form. The PDWG method employs locally reconstructed differential operators and stabilizers in the weak Galerkin framework, and yields a symmetric discrete linear system involving the primal variable and the dual variable (known as the Lagrangian multiplier) for the adjoint equation. Optimal order error estimates are established in various discrete Sobolev norms for the corresponding numerical solutions. Numerical results are reported to illustrate the accuracy and efficiency of the new PDWG method.

© 2022 Elsevier B.V. All rights reserved.

1. Introduction

This paper is concerned with the development of a symmetric numerical method for first order transport equations in non-divergence form by using the primal-dual finite element framework presented in [1]. For simplicity, we consider the model problem that seeks an unknown function λ satisfying

$$\beta(x) \cdot \nabla \lambda - c(x)\lambda = f \quad \text{in } \Omega,$$

$$\lambda = g \quad \text{on } \Gamma_{-},$$
(1.1)

where Ω is an open bounded and connected domain in \mathbb{R}^d (d=2,3) with Lipschitz continuous boundary $\Gamma=\partial\Omega$, Γ_- is the inflow boundary satisfying $\boldsymbol{\beta}\cdot\mathbf{n}<0$, and \mathbf{n} is the unit outward normal direction to Γ . Assume that the convection

E-mail addresses: chunmei.wang@ufl.edu (C. Wang), jwang@nsf.gov (J. Wang).

^{*} Corresponding author.

¹ The research of Chunmei Wang was partially supported by National Science Foundation Award DMS-2136380.

² The research of Junping Wang was supported in part by the NSF IR/D program, while working at National Science Foundation. However, any opinion, finding, and conclusions or recommendations expressed in this material are those of the author and do not necessarily reflect the views of the National Science Foundation.

vector $\boldsymbol{\beta} = (\beta_1, \dots, \beta_d) \in [L^{\infty}(\Omega)]^d$ is piecewise smooth, the reaction coefficient $c \in L^{\infty}(\Omega)$ is piecewise continuous, the load function $f \in L^2(\Omega)$, and the inflow boundary data $g \in L^2(\Gamma)$.

The first-order transport equation arises in many areas of science and engineering. Numerical methods for transport equations often impose a mathematical and computational challenge on its stability and capability of resolving the solution's discontinuities or sharp changing fronts. The first order linear transport equation serves as a benchmark for testing new approaches in numerical partial differential equations. Readers are referred to the introduction section of [2] and the references cited therein for a detailed description of the first-order transport equation as well as its physical and engineering applications.

This paper will develop a new numerical method for the linear transport problem (1.1) where the convection vector $\boldsymbol{\beta}$ and the reaction coefficient c are assumed to be piecewise continuous functions without any coercivity assumption in the form of $c+\frac{1}{2}\nabla\cdot\boldsymbol{\beta}\geq\alpha>0$ or alike used in most existing literatures. Our new numerical scheme is devised by using the framework of the primal-dual weak Galerkin (PDWG) finite element method [1–13]. The PDWG method was originally formulated as a constraint optimization problem in which the "discontinuity" of the approximating solution is minimized with the constraint of a satisfaction of the PDE locally on each element. The idea of primal-dual for solving PDEs has been also developed by Burman [14,15] in other finite element contexts, and it was given the name of "stabilized finite element methods" by Burman.

The transport Eq. (1.1) can be viewed as the adjoint of a transport equation in divergence form [2]. In [2], the linear transport equation in divergence form was formulated into a weak form through the integration by parts so that no derivatives are applied to the primal variable. The corresponding numerical scheme thus has convergence under the H^{θ} -regularity assumption for the exact solution. For the transport equation in non-divergence form (1.1), we shall use a straightforward weak form through a simple test against any square integrable functions. Compared with [2], a stabilization term in the form of $\tau_2 \sum_{T \in \mathcal{T}_h} h_T^2(u_h, v)$ is introduced in the present PDWG scheme in order to achieve an optimal order of convergence in L^2 . In addition, a term $\sum_{T \in \mathcal{T}_h} \tau_1(f, \beta \cdot \nabla \sigma_0 - c\sigma_0)$ is added to the right-hand side of the dual equation to accommodate a least squares term in the stabilizer $s(\cdot, \cdot)$ for the dual equation. In other words, the PDWG scheme for the model problem (1.1) requires some non-trivial modifications of the numerical method presented in [2].

The main contributions of this paper are the following. First, a new PDWG numerical method was devised and analyzed mathematically for its solvability and stability. Secondly, a convergence was established based on a minimal assumption on the PDE coefficients; namely, the model problem has one and only one solution and the coefficients are merely piecewise smooth. It should be pointed out that, due to the non-smoothness of the convection vector β , the transport equation in non-divergence form cannot be formulated into a divergence form for an application of the scheme developed in [2].

The paper is organized as follows. In Section 2, we present a PDWG algorithm. In Section 3, we prove the existence and uniqueness for the numerical solution. In Section 4, we derive error equations for the PDWG finite element method. Sections Section 5 is devoted to a convergence analysis for the PDWG approximations. Section 6 contains a series of numerical results that demonstrate the efficiency, stability, and accuracy of the new PDWG method.

2. Primal-dual weak Galerkin algorithm

The usual notations for Sobolev spaces and norms are adopted in this article. For an open bounded domain $D \subset \mathbb{R}^d$ with Lipschitz continuous boundary, denote by $\|\cdot\|_{s,D}$, $|\cdot|_{s,D}$, and $(\cdot,\cdot)_{s,D}$ the norm, seminorm and the inner product in the Sobolev space $H^s(D)$, $s \geq 0$, respectively. $H^0(D)$ coincides with $L^2(D)$, and the norm and the inner product are denoted as $\|\cdot\|_D$ and $(\cdot,\cdot)_D$. When $D=\Omega$ or the domain of integration is clear from the context, the subscript D will be omitted in the norm and inner product notations. Denote by I the identity operator.

Denote by T a polygonal or polyhedral element with boundary ∂T . By a weak function on T, we mean a pair $v = \{v_0, v_b\}$ such that $v_0 \in L^2(T)$ and $v_b \in L^2(\partial T)$; v_0 can be viewed as the value of v in T and v_b represents v on ∂T . Let $\mathcal{W}(T)$ be the local space of all weak functions on T; i.e.,

$$W(T) = \{v = \{v_0, v_h\} : v_0 \in L^2(T), v_h \in L^2(\partial T)\}.$$

Let $P_r(T)$ be the space of polynomials on T with degree r and less. The discrete weak gradient of v, denoted as $\nabla_{w,r,T}v \in [P_r(T)]^d$ for $v \in \mathcal{W}(T)$, is defined by

$$(\nabla_{w,r,T}v, \boldsymbol{\psi})_T = -(v_0, \nabla \cdot \boldsymbol{\psi})_T + \langle v_b, \boldsymbol{\psi} \cdot \mathbf{n} \rangle_{\partial T}, \quad \forall \boldsymbol{\psi} \in [P_r(T)]^d. \tag{2.1}$$

From the integration by parts, (2.1) maybe rewritten as follows

$$(\nabla_{w,r,T}v, \boldsymbol{\psi})_T = (\nabla v_0, \boldsymbol{\psi})_T - (v_0 - v_b, \boldsymbol{\psi} \cdot \mathbf{n})_{\partial T}, \quad \forall \boldsymbol{\psi} \in [P_r(T)]^d, \tag{2.2}$$

provided that $v_0 \in H^1(T)$.

Let \mathcal{T}_h be a finite element partition of the domain Ω into polygons in 2D or polyhedra in 3D which is shape regular in the sense of [16]. Denote by \mathcal{E}_h the set of all edges/faces in \mathcal{T}_h , and $\mathcal{E}_h^0 = \mathcal{E}_h \setminus \partial \Omega$ the set of all interior edges/faces. Denote by h_T the size of $T \in \mathcal{T}_h$ and $h = \max_{T \in \mathcal{T}_h} h_T$ the meshsize of the partition \mathcal{T}_h . For any piecewise smooth function ϕ with respect to the partition \mathcal{T}_h , denote by $[\![\phi]\!]$ the jump of ϕ along the interior edge/face e given by

$$[\![\phi]\!] = \phi_1 \mathbf{n}_1 + \phi_2 \mathbf{n}_2,$$

where $\phi_i := \phi|_{T_i}$, and \mathbf{n}_i is the unit outward normal direction on $e = \partial T_1 \cap \partial T_2$ relative to the element T_i , i = 1, 2. Let $k \ge 1$ be a given integer. Denote by $W_k(T)$ the local space of discrete weak functions; i.e.,

$$W_{k}(T) = \{ \{\sigma_{0}, \sigma_{b}\} : \sigma_{0} \in P_{k}(T), \sigma_{b} \in P_{k}(e), e \subset \partial T \}.$$
 (2.3)

The global weak finite element space W_h can be obtained by patching $W_k(T)$ over all elements $T \in \mathcal{T}_h$ through a common value v_b on \mathcal{E}_h^0 . Denote by W_h^0 the subspace of W_h with vanishing boundary values on Γ_- ; i.e.,

$$W_h^0 = \{ \{ \sigma_0, \sigma_b \} \in W_h : \sigma_b |_e = 0, e \subset \Gamma_- \}.$$

Our second finite element space M_h consists of piecewise polynomials of degree m(k); i.e.,

$$M_h = \{w : w|_T \in P_{m(k)}(T), \forall T \in \mathcal{T}_h\},$$
 (2.4)

where m(k) = k - 1, or k.

For simplicity, denote by $\nabla_w \sigma$ the discrete weak gradient $\nabla_{w,k-1,T} \sigma$ computed by (2.1) on each element T; i.e.,

$$(\nabla_w \sigma)|_T = \nabla_{w,k-1,T}(\sigma|_T), \quad \forall T \in \mathcal{T}_h.$$

Introduce the following bilinear forms:

$$s(\rho, \sigma) = \sum_{T \in \mathcal{T}_h} \int_{\partial T} h_T^{-1}(\rho_0 - \rho_b)(\sigma_0 - \sigma_b) ds + \tau_1 \int_T (\boldsymbol{\beta} \cdot \nabla \rho_0 - c \rho_0)(\boldsymbol{\beta} \cdot \nabla \sigma_0 - c \sigma_0) dT,$$
(2.5)

$$b(\sigma, v) = \sum_{T \in \mathcal{T}_h} (\boldsymbol{\beta} \cdot \nabla_w \sigma - c \sigma_0, v)_T,$$

for any ρ , $\sigma \in W_h$, $v \in M_h$, where $\tau_1 \ge 0$ is a parameter.

The primal-dual weak Galerkin scheme for (1.1) can be stated as follows:

Primal-Dual Weak Galerkin Algorithm 2.1. Find $(\lambda_h; u_h) \in W_h \times M_h$, such that $\lambda_h|_e = Q_h(g|_e)$, $e \subset \Gamma_-$, and satisfying

$$s(\lambda_h, \sigma) + b(\sigma, u_h) = \sum_{T \in T_h} \tau_1(f, \boldsymbol{\beta} \cdot \nabla \sigma_0 - c\sigma_0)_T, \quad \forall \sigma \in W_h^0,$$
(2.6)

$$s(\lambda_h, \sigma) + b(\sigma, u_h) = \sum_{T \in T_h} \tau_1(f, \boldsymbol{\beta} \cdot \nabla \sigma_0 - c\sigma_0)_T, \quad \forall \sigma \in W_h^0,$$

$$-\tau_2 \sum_{T \in \mathcal{T}_h} h_T^2(u_h, v)_T + b(\lambda_h, v) = (f, v), \quad \forall v \in M_h,$$

$$(2.6)$$

where $\tau_2 > 0$ is a parameter and Q_b is the local L^2 projection operator into $P_k(e)$.

3. Solution existence and uniqueness

Denote by Q_0 the L^2 projection operator onto $P_k(T)$. Analogously, for $e \subset \partial T$, denote by Q_b the L^2 projection operator onto $P_k(e)$. The composite projection $Q_h w$ for $w \in H^1(\Omega)$ is given by

$$(Q_h w)|_T := \{Q_0(w|_T), Q_h(w|_{\partial T})\}, \quad \forall T \in \mathcal{T}_h.$$

Let Q_h be the L^2 projection operator onto the finite element space M_h . Denote by \mathbb{Q}_h the L^2 projection operator onto the space of piecewise polynomials of degree k-1. Observe that Q_h is identical to \mathbb{Q}_h when m(k)=k-1. The following commutative property is known [16]:

$$\nabla_w(Q_h w) = \mathbb{Q}_h(\nabla w), \qquad \forall w \in H^1(T). \tag{3.1}$$

For simplicity of analysis, in what follows in the paper, we assume that the convection vector $oldsymbol{eta}$ and the reaction coefficient c are piecewise continuous functions with respect to the finite element partition \mathcal{T}_h .

Theorem 3.1. Assume that the transport problem (1.1) has a unique solution. Then, the primal-dual weak Galerkin algorithm (2.6)–(2.7) has a unique solution for any parameter $\tau_1 > 0$.

Proof. It suffices to show that the homogeneous problem of (2.6)–(2.7) has only the trivial solution. To this end, assume f=0 and g=0. By choosing $v=u_h$ and $\sigma=\lambda_h$ in (2.6)–(2.7) we arrive at

$$s(\lambda_h, \lambda_h) + \tau_2 \sum_{T \in \mathcal{T}_h} h_T^2(u_h, u_h)_T = 0,$$

which implies $\lambda_0 = \lambda_b$ on each ∂T , $\boldsymbol{\beta} \cdot \nabla \lambda_0 - c\lambda_0 = 0$, and $u_h = 0$ on each element T. We thus obtain $\lambda_0 \in C^0(\Omega)$ and furthermore $\beta \cdot \nabla \lambda_0 - c\lambda_0 = 0$ in Ω , which, together with $\lambda_0 = \lambda_b = 0$ on Γ , yields $\lambda_0 \equiv 0$ in Ω from the solution uniqueness of the model problem (1.1). From $\lambda_0 = \lambda_b$ on each ∂T , we have $\lambda_b \equiv 0$ in Ω so that $\lambda_h \equiv 0$ in Ω . This completes the proof of the theorem. \square

Next, we shall study the solution uniqueness for the algorithm (2.6)–(2.7) when the least-squares term disappears from the stabilizer $s(\rho, \sigma)$ in (2.5). The linear transport operator in (1.1) is said to have the L^2 -regularity if there exists a constant C_1 such that the solution Φ of the following problem

$$\beta(x) \cdot \nabla \Phi - c(x)\Phi = F \quad \text{in } \Omega,$$

$$\lambda = 0 \quad \text{on } \Gamma$$
(3.2)

satisfies the following estimate

$$\|\Phi\|_0 \le C_1 \|F\|_0. \tag{3.3}$$

Theorem 3.2. Assume that β is locally $C^{1,\alpha}(T)$ and c is locally $C^{0,\alpha}(T)$ on each element $T \in \mathcal{T}_h$. Under the assumption of the L^2 -regularity estimate (3.3), the primal–dual weak Galerkin algorithm (2.6)–(2.7) with m(k) = k has one and only one solution with parameter value $\tau_1 = 0$ in (2.5), provide that the meshsize h is sufficiently small.

Proof. It suffices to show that the homogeneous problem of (2.6)–(2.7) has only the trivial solution. To this end, assume f=0 and g=0. As $\tau_1=0$, by choosing $v=u_h$ and $\sigma=\lambda_h$ in (2.6)–(2.7) we arrive at

$$s(\lambda_h, \lambda_h) + \tau_2 \sum_{T \in \mathcal{T}_h} h_T^2(u_h, u_h)_T = 0,$$

which leads to $\lambda_0 = \lambda_b$ on each ∂T and $u_h = 0$ on each element $T \in \mathcal{T}_h$. It follows from (2.7) that

$$\begin{aligned} 0 &= b(\lambda_h, v) \\ &= \sum_{T \in \mathcal{T}_h} (\boldsymbol{\beta} \cdot \nabla_w \lambda_h - c\lambda_0, v)_T \\ &= \sum_{T \in \mathcal{T}_h} (\boldsymbol{\beta} \cdot \nabla \lambda_0 - c\lambda_0, v)_T \\ &= \sum_{T \in \mathcal{T}_h} (\mathcal{Q}_h(\boldsymbol{\beta} \cdot \nabla \lambda_0 - c\lambda_0), v)_T \end{aligned}$$

for all $v \in M_h$, where we have used $\nabla_w \lambda_h = \nabla \lambda_0$ due to the fact that $\lambda_0 = \lambda_b$ on each ∂T . Thus, we have $\mathcal{Q}_h(\boldsymbol{\beta} \cdot \nabla \lambda_0 - c\lambda_0) = 0$ on each $T \in \mathcal{T}_h$. From $\lambda_0 = \lambda_b$ on each ∂T we have $\lambda_0 \in C^0(\Omega)$ so that

$$\boldsymbol{\beta} \cdot \nabla \lambda_0 - c\lambda_0 = (I - \mathcal{Q}_h)(\boldsymbol{\beta} \cdot \nabla \lambda_0 - c\lambda_0) := F, \quad \lambda_0|_{\Gamma_-} = 0. \tag{3.4}$$

From the L^2 -regularity assumption (3.3), Eq. (3.4), and the assumption of m(k) = k, we arrive at

$$\begin{split} \|\lambda_0\|_0 &\leq C_1 \|F\|_0 \\ &\leq C_1 \Big(\sum_{T \in \mathcal{T}_h} \|(I - \mathcal{Q}_h)(\boldsymbol{\beta} \cdot \nabla \lambda_0 - c\lambda_0)\|_T^2 \Big)^{\frac{1}{2}} \\ &\leq C_1 \Big(\sum_{T \in \mathcal{T}} \|(I - \mathcal{Q}_h)((\boldsymbol{\beta} - \tilde{\boldsymbol{\beta}}) \cdot \nabla \lambda_0)\|_T^2 + \|(I - \mathcal{Q}_h)((\boldsymbol{c} - \overline{\boldsymbol{c}})\lambda_0)\|_T^2 \Big)^{\frac{1}{2}}, \end{split}$$

where $\tilde{\beta}$ is the L^2 projection of β onto the space of piecewise linear functions and \bar{c} is the L^2 projection of c onto the space of piecewise constant functions. Since β is locally $C^{1,\alpha}$ and c is locally $C^{0,\alpha}$, we thus have

$$\|\lambda_{0}\|_{0} \leq C_{1} \left(\sum_{T \in \mathcal{T}_{h}} \|\boldsymbol{\beta} - \tilde{\boldsymbol{\beta}}\|_{L^{\infty}(T)}^{2} \|\nabla \lambda_{0}\|_{0,T}^{2} + \|c - \overline{c}\|_{L^{\infty}(T)}^{2} \|\lambda_{0}\|_{0,T}^{2} \right)^{\frac{1}{2}}$$

$$\leq C_{1} \left(C_{2} h_{T}^{2+2\alpha} \sum_{T \in \mathcal{T}_{h}} \|\nabla \lambda_{0}\|_{0,T}^{2} + C_{3} h_{T}^{2\alpha} \|\lambda_{0}\|_{0,T}^{2} \right)^{\frac{1}{2}}$$

$$\leq C h^{\alpha} \|\lambda_{0}\|_{0,T}^{2}$$

where we have used the inverse inequality in the last estimate. Hence

$$(1-Ch^{\alpha})\|\lambda_0\|_0\leq 0,$$

which leads to $\|\lambda_0\|_0 = 0$ when the meshsize h is sufficiently small. This shows that $\lambda_0 \equiv 0$ in Ω , and furthermore, $\lambda_b \equiv 0$ from the fact that $\lambda_b = \lambda_0$ on each ∂T . This completes the proof of the theorem. \Box

4. Error equations

Let λ be the exact solution of the transport problem (1.1) and $(\lambda_h, u_h) \in W_h \times M_h$ be its numerical approximation arising from the scheme (2.6)–(2.7). Denote the error functions by

$$\epsilon_h = \lambda_h - Q_h \lambda,$$
 (4.1)

$$e_h = u_h - Q_h u. \tag{4.2}$$

Note that the exact solution to the dual equation is the trivial function u = 0.

Lemma 4.1. The error functions ϵ_h and e_h satisfy the following equations:

$$s(\epsilon_h, \sigma) + b(\sigma, e_h) = \ell_{\lambda}(\sigma), \quad \forall \sigma \in W_h^0,$$
 (4.3)

$$-\tau_2 \sum_{T \in \mathcal{T}_h} h_T^2(e_h, v)_T + b(\epsilon_h, v) = \zeta_\lambda(v), \qquad \forall v \in M_h.$$

$$(4.4)$$

Here,

$$\ell_{\lambda}(\sigma) = \sum_{T \in \mathcal{T}_{h}} \tau_{1}(\boldsymbol{\beta} \cdot \nabla(\lambda - Q_{0}\lambda) - c(\lambda - Q_{0}\lambda), \, \boldsymbol{\beta} \cdot \nabla\sigma_{0} - c\sigma_{0})_{T}$$

$$- h_{T}^{-1} \langle Q_{0}\lambda - Q_{b}\lambda, \, \sigma_{0} - \sigma_{b}\rangle_{\partial T},$$

$$(4.5)$$

$$\zeta_{\lambda}(v) = \sum_{T \in \mathcal{T}_{h}} (\boldsymbol{\beta} \cdot (I - \mathbb{Q}_{h}) \nabla \lambda - c(\lambda - Q_{0}\lambda), v)_{T}.$$

$$(4.6)$$

Proof. From (2.7) and the commutative property (3.1) we have

$$-\tau_{2} \sum_{T \in \mathcal{T}_{h}} h_{T}^{2}(u_{h} - \mathcal{Q}_{h}u, v)_{T} + b(\lambda_{h} - Q_{h}\lambda, v)$$

$$= (f, v) - b(Q_{h}\lambda, v)$$

$$= (f, v) - \sum_{T \in \mathcal{T}_{h}} (\boldsymbol{\beta} \cdot \nabla_{w}Q_{h}\lambda - cQ_{0}\lambda, v)_{T}$$

$$= (\boldsymbol{\beta} \cdot \nabla\lambda - c\lambda, v) - \sum_{T \in \mathcal{T}_{h}} (\boldsymbol{\beta} \cdot Q_{h}\nabla\lambda - cQ_{0}\lambda, v)_{T}$$

$$= \sum_{T \in \mathcal{T}_{h}} (\boldsymbol{\beta} \cdot (I - Q_{h})\nabla\lambda - c(\lambda - Q_{0}\lambda), v)_{T},$$

where we have used the first equation in (1.1), which gives (4.4). To derive (4.3), we subtract $s(Q_h\lambda, \sigma)$ from both sides of (2.6) to obtain

$$\begin{split} &s(\lambda_h - Q_h \lambda, \sigma) + b(\sigma, u_h - Q_h u) \\ &= \sum_{T \in \mathcal{T}_h} \tau_1(f, \boldsymbol{\beta} \cdot \nabla \sigma_0 - c\sigma_0)_T - s(Q_h \lambda, \sigma) \\ &= \sum_{T \in \mathcal{T}_h} \tau_1(\boldsymbol{\beta} \cdot \nabla \lambda - c\lambda, \boldsymbol{\beta} \cdot \nabla \sigma_0 - c\sigma_0)_T - h_T^{-1} \langle Q_0 \lambda - Q_b \lambda, \sigma_0 - \sigma_b \rangle_{\partial T} \\ &- \tau_1(\boldsymbol{\beta} \cdot \nabla Q_0 \lambda - cQ_0 \lambda, \boldsymbol{\beta} \cdot \nabla \sigma_0 - c\sigma_0)_T \\ &= \sum_{T \in \mathcal{T}_h} \tau_1(\boldsymbol{\beta} \cdot \nabla (\lambda - Q_0 \lambda) - c(\lambda - Q_0 \lambda), \boldsymbol{\beta} \cdot \nabla \sigma_0 - c\sigma_0)_T \\ &- h_T^{-1} \langle Q_0 \lambda - Q_b \lambda, \sigma_0 - \sigma_b \rangle_{\partial T}, \end{split}$$

which leads to the error Eq. (4.3). This completes the proof of the lemma. \Box

5. Error estimates

Introduce a scaled L^2 norm in the finite element space M_h as follows:

$$|||v||_{M_h} = \left(\tau_2 \sum_{T \in \mathcal{T}_h} h_T^2 ||v||_T^2\right)^{\frac{1}{2}}, \qquad v \in M_h,$$
(5.1)

where $\tau_2 > 0$. In W_h , we equip the following semi-norm:

$$\|\|\lambda\|_{W_h} = \left(\sum_{T \in \mathcal{T}_h} h_T^{-1} \|\lambda_0 - \lambda_b\|_{\partial T}^2 + \tau_1 \|\boldsymbol{\beta} \cdot \nabla \lambda_0 - c\lambda_0\|_T^2\right)^{\frac{1}{2}},\tag{5.2}$$

where $\tau_1 \geq 0$.

Lemma 5.1. Assume that the solution to the transport problem in the non-divergence form (1.1) is unique. Then the seminorm $\|\cdot\|_{W_h}$ defines a norm in the linear space W_h^0 when $\tau_1 > 0$.

Proof. We shall only verify the positivity property for $\|\cdot\|_{W_h}$. To this end, assume $\|\lambda\|_{W_h} = 0$ for some $\lambda = \{\lambda_0, \lambda_b\} \in W_h^0$. Since $\tau_1 > 0$, then from (5.2) we have $\lambda_0 = \lambda_b$ on ∂T and $\boldsymbol{\beta} \cdot \nabla \lambda_0 - c\lambda_0 = 0$ on any $T \in \mathcal{T}_h$. This implies $\lambda_0 \in C^0(\Omega)$ and $\boldsymbol{\beta} \cdot \nabla \lambda_0 - c\lambda_0 = 0$ in Ω . Thus, from $\lambda \in W_h^0$ and the solution uniqueness for (1.1) we obtain $\lambda_0 \equiv 0$ and furthermore, $\lambda_b = \lambda_0 = 0$. This completes the proof of the lemma. \square

Recall that \mathcal{T}_h is a shape-regular finite element partition of the domain Ω . Thus, for any $T \in \mathcal{T}_h$ and $\phi \in H^1(T)$, the following trace inequality holds true [16]:

$$\|\phi\|_{\partial T}^2 \le C(h_T^{-1}\|\phi\|_T^2 + h_T\|\nabla\phi\|_T^2). \tag{5.3}$$

If ϕ is a polynomial on the element $T \in \mathcal{T}_h$, the following trace inequality holds true [16]; i.e.,

$$\|\phi\|_{\partial T}^2 \le Ch_T^{-1} \|\phi\|_T^2. \tag{5.4}$$

Lemma 5.2 ([16]). Let \mathcal{T}_h be a finite element partition of the domain Ω satisfying the shape regular assumption as specified in [16]. For any $0 \le s \le 1$ and $0 \le m \le k$, there holds

$$\sum_{T \in \mathcal{T}_{k}} h_{T}^{2s} \|u - \mathcal{Q}_{h} u\|_{s,T}^{2} \le C h^{2n+2} \|u\|_{n+1}^{2}, \quad 0 \le n \le m(k),$$

$$(5.5)$$

$$\sum_{T \in \mathcal{T}} h_T^{2s} \|\lambda - Q_0 \lambda\|_{s,T}^2 \le C h^{2m+2} \|\lambda\|_{m+1}^2, \quad 0 \le m \le k.$$
 (5.6)

Theorem 5.3. Let λ and $(\lambda_h; u_h) \in W_h \times M_h$ be the exact solution of the transport problem (1.1) and the primal–dual weak Galerkin solution arising from the numerical scheme (2.6)–(2.7), respectively. Assume that the exact solution λ is sufficiently regular such that $\lambda \in \bigoplus_{j=1}^J H^{k+1}(\Omega_j)$ where $\{\Omega_j\}_{j=1}^J$ is a non-overlapping partition of the domain Ω . Then, the following estimate holds true:

$$\|\|\epsilon_h\|_{W_h} + \|\|e_h\|_{M_h} \le C(1 + \tau_2^{-\frac{1}{2}})h^k \sum_{i=1}^J \|\lambda\|_{k+1,\Omega_j}.$$
(5.7)

Proof. By setting $\sigma = \epsilon_h$ in the error Eq. (4.3) and $v = e_h$ in (4.4), we have

$$\tau_2 \sum_{T \in \mathcal{T}_h} h_T^2(e_h, e_h)_T + s(\epsilon_h, \epsilon_h) = \ell_{\lambda}(\epsilon_h) - \zeta_{\lambda}(e_h),$$

which gives

$$|||e_h||_{M_h}^2 + |||\epsilon_h||_{W_h}^2 \le |\ell_\lambda(\epsilon_h)| + |\zeta_\lambda(e_h)| = I_1 + I_2.$$
(5.8)

We shall estimate the two terms I_1 and I_2 in (5.8). For I_1 , it follows from the Cauchy–Schwarz inequality, the triangle inequality, (4.5), the trace inequality (5.3), and the estimate (5.6) with m = k that

$$\begin{split} I_{1} &= \left| \sum_{T \in \mathcal{T}_{h}} \tau_{1}(\boldsymbol{\beta} \cdot \nabla(\lambda - Q_{0}\lambda) - c(\lambda - Q_{0}\lambda), \boldsymbol{\beta} \cdot \nabla \epsilon_{0} - c\epsilon_{0})_{T} \right. \\ &- h_{T}^{-1}(Q_{0}\lambda - Q_{b}\lambda, \epsilon_{0} - \epsilon_{b})_{\partial T} \Big| \\ &\leq \left(\left(\sum_{T \in \mathcal{T}_{h}} \tau_{1} \| \boldsymbol{\beta} \cdot \nabla(\lambda - Q_{0}\lambda) \|_{T}^{2} \right)^{\frac{1}{2}} + \left(\sum_{T \in \mathcal{T}_{h}} \tau_{1} \| c(\lambda - Q_{0}\lambda) \|_{T}^{2} \right)^{\frac{1}{2}} \right) \\ &\cdot \left(\sum_{T \in \mathcal{T}_{h}} \tau_{1} \| \boldsymbol{\beta} \cdot \nabla \epsilon_{0} - c\epsilon_{0} \|_{T}^{2} \right)^{\frac{1}{2}} + \left(\sum_{T \in \mathcal{T}_{h}} h_{T}^{-1} \| \epsilon_{0} - \epsilon_{b} \|_{\partial T}^{2} \right)^{\frac{1}{2}} \left(\sum_{T \in \mathcal{T}_{h}} h_{T}^{-1} \| Q_{0}\lambda - Q_{b}\lambda \|_{\partial T}^{2} \right)^{\frac{1}{2}} \\ &+ \left(\sum_{T \in \mathcal{T}_{h}} h_{T}^{-1} \| \epsilon_{0} - \epsilon_{b} \|_{\partial T}^{2} \right)^{\frac{1}{2}} \left(\sum_{T \in \mathcal{T}_{h}} h_{T}^{-1} \| Q_{0}\lambda - Q_{b}\lambda \|_{\partial T}^{2} \right)^{\frac{1}{2}} \\ &\leq \|\epsilon_{h}\|_{W_{h}} \left(Ch^{k} \sum_{j=1}^{J} \|\lambda\|_{k+1,\Omega_{j}} + Ch^{k+1} \sum_{j=1}^{J} \|\lambda\|_{k+1,\Omega_{j}} \right) \\ &+ \|\epsilon_{h}\|_{W_{h}} \left(Ch^{k} \sum_{j=1}^{J} \|\lambda\|_{k+1,\Omega_{j}} + C(\sum_{T \in \mathcal{T}_{h}} h_{T}^{-2} \|Q_{0}\lambda - \lambda\|_{T}^{2} + \|Q_{0}\lambda - \lambda\|_{1,T}^{2} \right)^{\frac{1}{2}} \right) \\ &\leq Ch^{k} \|\epsilon_{h}\|_{W_{h}} \sum_{j=1}^{J} \|\lambda\|_{k+1,\Omega_{j}}. \end{split}$$

As to I_2 , we use the orthogonality property of Q_h to obtain

$$\begin{split} I_2 &= \bigg| \sum_{T \in \mathcal{T}_h} (\boldsymbol{\beta} \cdot (I - \mathbb{Q}_h) \nabla \lambda - c(\lambda - Q_0 \lambda), e_h)_T \bigg| \\ &\leq \bigg| \sum_{T \in \mathcal{T}_h} (\boldsymbol{\beta} \cdot (I - \mathbb{Q}_h) \nabla \lambda, e_h)_T \bigg| + \bigg| \sum_{T \in \mathcal{T}_h} (c(\lambda - Q_0 \lambda), e_h)_T \\ &= \bigg| \sum_{T \in \mathcal{T}_h} ((I - \mathbb{Q}_h) \nabla \lambda, (I - \mathbb{Q}_h) (\boldsymbol{\beta} - \overline{\boldsymbol{\beta}}) e_h)_T \bigg| \\ &+ \bigg| \sum_{T \in \mathcal{T}} (\lambda - Q_0 \lambda, c e_h)_T \bigg|. \end{split}$$

Next, from the Cauchy–Schwarz inequality, (4.6), the triangle inequality, the estimate (5.5) with m = k and m = 1, the estimate (5.6) with m = k, and the inverse inequality we obtain

$$|I_{2}| \leq \left(\sum_{T \in \mathcal{T}_{h}} \|(I - \mathbb{Q}_{h})\nabla\lambda\|_{T}^{2}\right)^{\frac{1}{2}} \left(\sum_{T \in \mathcal{T}_{h}} \|(I - \mathbb{Q}_{h})(\boldsymbol{\beta} - \overline{\boldsymbol{\beta}})e_{h}\|_{T}^{2}\right)^{\frac{1}{2}}$$

$$+ \|c\|_{L^{\infty}(\Omega)} \left(\sum_{T \in \mathcal{T}_{h}} \tau_{2}^{-1}h_{T}^{-2}\|Q_{0}\lambda - \lambda\|_{T}^{2}\right)^{\frac{1}{2}} \left(\sum_{T \in \mathcal{T}_{h}} \tau_{2}h_{T}^{2}\|e_{h}\|_{T}^{2}\right)^{\frac{1}{2}}$$

$$\leq C_{1}h^{k} \left(\left(\sum_{T \in \mathcal{T}_{h}} h_{T}^{2}\|\nabla(\boldsymbol{\beta} - \overline{\boldsymbol{\beta}})e_{h}\|_{0,T}^{2}\right)^{\frac{1}{2}} + C_{2}\tau_{2}^{-\frac{1}{2}} \|e_{h}\|_{M_{h}}\right) \sum_{j=1}^{J} \|\lambda\|_{k+1,\Omega_{j}}$$

$$\leq C\tau_{2}^{-\frac{1}{2}}h^{k} \|e_{h}\|_{M_{h}} \sum_{j=1}^{J} \|\lambda\|_{k+1,\Omega_{j}},$$

$$(5.10)$$

where we have used the fact that $\max_{T \in \mathcal{T}_h} \|\nabla \boldsymbol{\beta}\|_{L^{\infty}(T)} \leq C$ due to the piecewise smoothness assumption on $\boldsymbol{\beta}$ with respect to the finite element partition \mathcal{T}_h .

Combining (5.8) with (5.9) and (5.10) yields the error estimate (5.7). This completes the proof of the theorem. \Box

6. Numerical experiments

In this section we shall report some computational results for the scheme (2.6)–(2.7) with linear and quadratic elements (i.e., k = 1, 2). Recall that the finite element spaces are constructed as follows

$$W_h^{(k)} = \{ \{\lambda_0, \lambda_b\} : \lambda_0 \in P_k(T), \lambda_b \in P_k(e), e \subset \partial T, \forall T \in \mathcal{T}_h \},$$

$$M_h^{(k)} = \{ u_h : u_h|_T \in P_{m(k)}(T), \ \forall T \in \mathcal{T}_h \}, \quad m(k) = k - 1, \text{ or } k.$$

For convenience, they are referred to as $C^{-1} - P_k(T)/P_k(\partial T)/P_{m(k)}(T)$ element in this section. The numerical solution $\lambda_h = \{\lambda_0, \lambda_b\} \in W_h^{(k)}$ and $u_h \in M_h^{(k)}$ is compared with the L^2 projection of the exact solution λ and u = 0. The corresponding error functions are denoted as

$$\epsilon_0 = \lambda_0 - Q_0 \lambda$$
, $\epsilon_b = \lambda_b - Q_b \lambda$, $e_h = u_h - Q_h u = u_h$.

The L^2 norm for the error λ_h on the element boundary is defined as

$$\|\epsilon_b\| = \left(\sum_{T \in \mathcal{T}_h} h_T \int_{\partial T} \epsilon_b^2 ds\right)^{\frac{1}{2}}.$$

The numerical experiments are conducted on several polygonal domains Ω_i . The first one is the unit square domain $\Omega_1 = (0, 1)^2$. The second one, denoted as Ω_2 , is an L-shaped domain with vertices $A_1 = (0, 0)$, $A_2 = (1, 0)$, $A_3 = (1, 0.5)$, $A_4 = (0.5, 0.5), A_5 = (0.5, 1), \text{ and } A_6 = (0, 1).$ The third one is a cracked unit square given by $\Omega_3 = (0, 1)^2 \setminus (0.5, 1) \times \{0.5\}.$ The crack clearly takes place along the edge $(0.5, 1) \times \{0.5\}$. Our fourth one is also a cracked diamond characterized as $\Omega_4 = \{(x, y) : |x| + |y| < 1\} \setminus \{(0, 1) \times 0\}$. The inflow boundary Γ_- is determined by the condition of $\beta \cdot \mathbf{n} < 0$, where **n** is the unit outward normal direction on $\partial \Omega$. The right-hand side function f and the inflow Dirichlet data g are set to match the exact solution λ if possible.

Our numerical experiments are based on uniform partitions of the domain, which are obtained through a successive refinement of a given coarse triangulation by dividing each coarse element into four congruent sub-triangles by connecting the mid-points on the three edges of the triangular element. The rectangular partitions are generated through a successive refinement of a coarse 3×2 rectangular partition of the domain by dividing each coarse element into four congruent sub-rectangles by connecting the mid-points on the two parallel edges.

6.1. Constant-valued convection vector $\boldsymbol{\beta}$

This test problem is defined on Ω_1 , with exact solution $\lambda = \cos(x)\cos(y)$, convection tensor $\beta = [1, 1]$, and reaction coefficient c = 1. Tables 6.1 and 6.2 illustrate the numerical performance of the $C^{-1} - P_1(T)/P_1(\partial T)/P_0(T)$ element when triangular and rectangular partitions are employed, respectively. Table 6.1 shows that the convergence for ϵ_0 and ϵ_b in the L^2 norm is of optimal order of $\mathcal{O}(h^2)$ on triangular partitions with $(\tau_1, \tau_2) = (0, 0)$. Table 6.2 suggests that the convergence for ϵ_0 and ϵ_b in the L^2 norm is also at the optimal order of $\mathcal{O}(h^2)$ on rectangular partitions, but a superconvergence is observed for the dual variable u_h on rectangular partitions.

Tables 6.3 and 6.4 illustrate the performance of numerical scheme when the $C^{-1} - P_2(T)/P_2(\partial T)/P_1(T)$ element are employed on the L-shaped domain Ω_2 . The exact solution is given by $\lambda = \cos(x)\cos(y)$, the convection vector is $\boldsymbol{\beta} = [1, 1]$,

Numerical rates of convergence for the $C^{-1} - P_1(T)/P_1(\partial T)/P_0(T)$ element with the exact solution $\lambda = \cos(x)\cos(y)$ on the unit square domain Ω_1 ; uniform triangular partitions; convection vector $\beta = [1, 1]$; reaction coefficient c = 1; and the parameters $(\tau_1, \tau_2) = (0, 0)$.

1/h	$\ \epsilon_0\ $	Order	$\ \epsilon_b\ $	Order	$\ e_h\ $	Order
4	1.0883E-02	2.0976	1.9684E-02	2.1808	1.1270E-02	0.6656
8	2.4728E-03	2.1379	4.3116E-03	2.1908	5.9859E-03	0.9128
16	5.6872E-04	2.1203	9.7480E-04	2.1450	3.0096E-03	0.9920
32	1.3458E-04	2.0793	2.2889E-04	2.0904	1.5017E-03	1.0030

Table 6.2 Numerical rates of convergence for the $C^{-1} - P_1(T)/P_1(\partial T)/P_0(T)$ element with the exact solution $\lambda = \cos(x)\cos(y)$ on the unit square domain Ω_1 ; uniform rectangular partitions; convection vector $\beta = [1, 1]$; reaction coefficient c = 1; and the parameters $(\tau_1, \tau_2) = (0, 0)$.

1/h	$\ \epsilon_0\ $	Order	$\ \epsilon_b\ $	Order	$\ e_h\ $	Order
4	5.3456E-03	1.8945	1.1620E-02	2.0765	1.8751E-03	0.2718
8	1.3145E-03	2.0238	2.5890E-03	2.1661	9.0089E - 04	1.0575
16	3.1893E-04	2.0432	5.8772E-04	2.1392	3.3841E-04	1.4126
32	7.7962E-05	2.0324	1.3796E-04	2.0909	1.1621E-04	1.5420

Table 6.3 Numerical rates of convergence for the $C^{-1} - P_2(T)/P_2(\partial T)/P_1(T)$ element with the exact solution $\lambda = \cos(x)\cos(y)$ on the L-shaped domain Ω_2 ; uniform triangular partitions; convection vector $\boldsymbol{\beta} = [1, 1]$; reaction coefficient c = 1; and the parameters $(\tau_1, \tau_2) = (0, 1)$.

1/h	$\ \epsilon_0\ $	Order	$\ \epsilon_b\ $	Order	$\ e_h\ $	Order
4	2.9682E-05	3.2140	6.1448E-05	3.1241	3.0201E-04	1.7985
8	3.3257E-06	3.1579	7.1909E-06	3.0951	8.0495E-05	1.9076
16	3.8296E-07	3.1184	8.5521E-07	3.0718	2.0782E-05	1.9536
32	4.5478E-08	3.0740	1.0369E-07	3.0441	5.2789E-06	1.9770

Table 6.4 Numerical rates of convergence for the $C^{-1} - P_2(T)/P_2(\partial T)/P_1(T)$ element with the exact solution $\lambda = \cos(x)\cos(y)$ on the L-shaped domain Ω_2 ; uniform triangular partitions; convection vector $\boldsymbol{\beta} = [1, 1]$; reaction coefficient c = 1; and the parameters $(\tau_1, \tau_2) = (0, 0)$.

1/h	$\ \epsilon_0\ $	Order	$\ \epsilon_b\ $	Order	$\ e_h\ $	Order
4	2.9790E-05	3.2274	6.1690E-05	3.1381	3.0360E-04	1.8214
8	3.3289E-06	3.1617	7.1986E-06	3.0993	8.0598E-05	1.9134
16	3.8306E-07	3.1194	8.5546E-07	3.0730	2.0789E-05	1.9549
32	4.5481E-08	3.0742	1.0369E-07	3.0444	5.2794E-04	1.9774

Table 6.5 Numerical rates of convergence for the $C^{-1} - P_2(T)/P_2(\partial T)/P_1(T)$ element with the exact solution $\lambda = \exp(x)\cos(y)$ on the cracked domain Ω_3 ; uniform triangular partitions; convection $\boldsymbol{\beta} = [0.5 - y, x - 0.5]$; reaction c = 0; and the parameters $(\tau_1, \tau_2) = (0, 0)$.

1/h	$\ \epsilon_0\ $	Order	$\ \epsilon_b\ $	Order	$\ e_h\ $	Order
4	9.1034E-05	3.4056	1.4755E-04	3.4116	4.9032E-03	2.0398
8	9.7249E - 06	3.2267	1.5660E-05	3.2360	1.3389E-03	1.8727
16	1.1326E-06	3.1021	1.7997E-06	3.1212	3.6043E-04	1.8933
32	1.3717E-07	3.0456	2.1528E-07	3.0635	9.6096E-05	1.9072

Table 6.6 Numerical rates of convergence for the $C^{-1} - P_2(T)/P_2(\partial T)/P_1(T)$ element with the exact solution $\lambda = \sin(\pi x)\cos(\pi y)$ on the unit square domain Ω_1 ; uniform triangular partitions; convection $\boldsymbol{\beta} = [-y, x]$; reaction c = x + y; and the parameters $(\tau_1, \tau_2) = (1, 0)$.

1/h	$\ \epsilon_0\ $	Order	$\ \epsilon_b\ $	Order	$\ e_h\ $	Order
4	1.8233E-02	3.2195	3.0485E-02	3.2969	4.8981E-01	2.0117
8	1.6511E-03	3.4651	2.6914E-03	3.5017	1.2298E-01	1.9938
16	1.6687E-04	3.3067	2.7016E-04	3.3165	3.1170E-02	1.9801
32	1.9382E-05	3.1059	3.0957E-05	3.1255	7.9248E-03	1.9757

and the reaction coefficient is c=1. The numerical results show that the convergence for ϵ_0 and ϵ_b in the L^2 norm are of the optimal order $\mathcal{O}(h^3)$.

6.2. Continuous convection vector $\boldsymbol{\beta}$

Table 6.5 demonstrates the numerical performance of the $C^{-1} - P_2(T)/P_2(\partial T)/P_1(T)$ element on the uniform triangular partition for the cracked domain Ω_3 . The exact solution is given as $\lambda = \exp(x)\cos(y)$, the convection is a circular $\beta = [0.5 - y, x - 0.5]$, and the reaction is c = 0. The numerical results show that the convergence for ϵ_0 and ϵ_b in the L^2 norm arrive at the optimal order of $\mathcal{O}(h^3)$.

Table 6.6 demonstrates the computational performance of the algorithm on the uniform triangular partition of the unit square domain Ω_1 . The exact solution is $\lambda = \sin(\pi x)\cos(\pi y)$, the convection is $\beta = [-y, x]$, and the reaction is c = x + y. The numerical results show that the convergence for ϵ_0 and ϵ_b in the L^2 norm are of the optimal order $\mathcal{O}(h^3)$ when the $C^{-1} - P_2(T)/P_2(\partial T)/P_1(T)$ element is used.

6.3. Discontinuous convection β

This numerical test was conducted for the $C^{-1} - P_1(T)/P_1(\partial T)/P_0(T)$ element on uniform triangular partitions for the unit square domain Ω_1 . The exact solution is given by $\lambda = \sin(x)\cos(y)$. The convection vector $\boldsymbol{\beta}$ is defined as $\boldsymbol{\beta} = [1, -1]$ for y < 1 - x and $\boldsymbol{\beta} = [-2, 2]$ otherwise. The reaction term is given by c = 1. The numerical results in Tables 6.7–6.8 show that the convergence for ϵ_0 and ϵ_b in the L^2 norm are of the optimal order $\mathcal{O}(h^2)$.

Fig. 6.1 shows the plots of the numerical solution λ_0 arising from the PDWG scheme (2.6)–(2.7) when the $C^{-1} - P_2(T)/P_2(\partial T)/P_1(T)$ element is employed. The configuration of the test problem is as follows: (1) the convection β

Table 6.7 Numerical rates of convergence for the $C^{-1} - P_1(T)/P_1(\partial T)/P_0(T)$ element with exact solution $\lambda = \sin(x)\cos(y)$ on the unit square domain Ω_1 ; uniform triangular partitions; convection $\boldsymbol{\beta} = [1, -1]$ for y < 1 - x and $\boldsymbol{\beta} = [-2, 2]$ otherwise; reaction c = 1; and the parameters $(\tau_1, \tau_2) = (0, 1)$.

1/h	$\ \epsilon_0\ $	Order	$\ \epsilon_b\ $	Order	$\ e_h\ $	Order
1	3.2120E-02		7.0574E-02		9.0720E-03	
2	1.1795E-02	1.4452	2.1695E-02	1.7018	2.3864E-03	1.9266
4	2.8507E-03	2.0489	4.9996E-03	2.1175	9.1523E-04	1.3826
8	7.0230E-04	2.0197	1.1936E-03	2.0664	4.2927E-04	1.0922
16	1.7520E-04	2.0045	2.9198E-04	2.0315	2.1125E-04	1.0229
32	4.3771E-05	2.0009	7.2224E-05	2.0153	1.0519E-04	1.0059

Table 6.8 Numerical rates of convergence for the $C^{-1} - P_1(T)/P_1(\partial T)/P_0(T)$ element with the exact solution $\lambda = \sin(x)\cos(y)$ on the unit square domain Ω_1 ; uniform triangular partitions; convection $\boldsymbol{\beta} = [1, -1]$ for y < 1 - x and $\boldsymbol{\beta} = [-2, 2]$ otherwise; reaction c = 1; and the parameters $(\tau_1, \tau_2) = (0, 0)$.

1/h	$\ \epsilon_0\ $	Order	$\ \epsilon_b\ $	Order	$\ e_h\ $	Order
1	4.0936E-02		9.0019E-02		1.3976E-02	_
2	1.2259E-02	1.7396	2.2582E-02	1.9951	3.0632E-03	2.1899
4	2.9157E-03	2.0719	5.1131E-03	2.1429	1.2530E-03	1.2896
8	7.1768E-04	2.0224	1.2183E-03	2.0693	5.9790E-04	1.0675
16	1.7876E-04	2.0053	2.9787E-04	2.0321	2.9519E-04	1.0183
32	4.4655E-05	2.0012	7.3676E-05	2.0154	1.4707E-04	1.0051

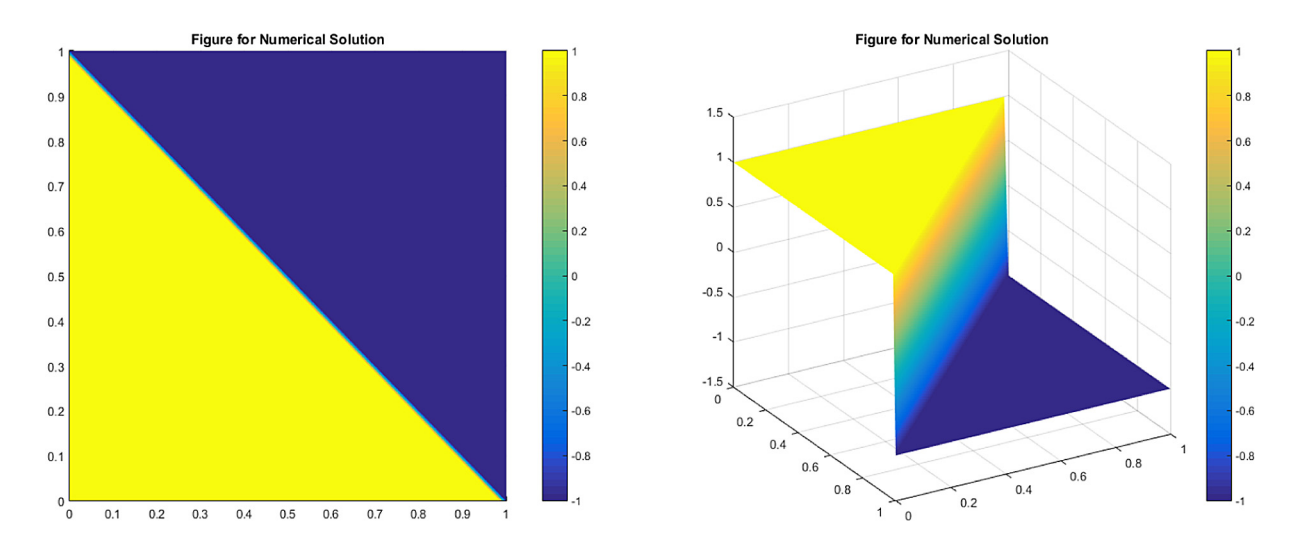


Fig. 6.1. Plots of numerical solution λ_0 on the unit square domain Ω_1 ; $C^{-1} - P_2(T)/P_2(\partial T)/P_1(T)$ element; uniform triangular partitions; convection $\beta = [1, -1]$ for y < 1 - x and $\beta = [-2, 2]$ elsewhere; reaction c = 0; the load function f = 0; the inflow boundary data g = 1 on the inflow boundary edge $\{0\} \times (0, 1)$ and g = -1 on the inflow boundary edge $\{1\} \times (0, 1)$; and $(\tau_1, \tau_2) = (1, 1)$.

[1, -1] for y < 1 - x and $\beta = [-2, 2]$ elsewhere; (2) the reaction c = 0; (3) the load function f = 0; and (4) inflow boundary data of g = 1. The left one in Fig, 6.1 is the contour plot of the numerical solution λ_0 ; and the right one is its surface plot. It is easy to see that the numerical solution λ_0 is consistent with the exact solution λ of the model problem (1.1).

6.4. Plots of numerical solutions λ_0

Fig. 6.2 shows the contour plots of the numerical solution λ_0 obtained by using the $C^{-1} - P_2(T)/P_2(\partial T)/P_1(T)$ element in Ω_1 . The convection vector is given by $\boldsymbol{\beta} = [-y,x]$ for y < 1-x and $\boldsymbol{\beta} = [1-y,x-1]$ otherwise. The reaction term is given by c = 0. The inflow boundary data $g = \sin(3x)\cos(5y)$. The parameters are $(\tau_1,\tau_2) = (1,1)$. Fig. 6.2 demonstrates the contour plots of the numerical solution λ_0 for the load function f = 1 (left figure) and f = 0 (right figure), respectively. Fig. 6.3 shows the contour plots of the numerical solution λ_0 on the L-shaped domain Ω_2 . The convection vector is given by $\boldsymbol{\beta} = [-1,1]$ for y < 0.5-x and $\boldsymbol{\beta} = [1,-1]$ elsewhere, and the reaction is c = 1. The inflow boundary data is $g = \sin(\pi x)\cos(\pi y)$. The parameters are set as $(\tau_1,\tau_2) = (1,1)$. The plot in left is for the load functions f = 1, and the one on right is for f = 0 with $C^{-1} - P_2(T)/P_2(\partial T)/P_1(T)$ elements.

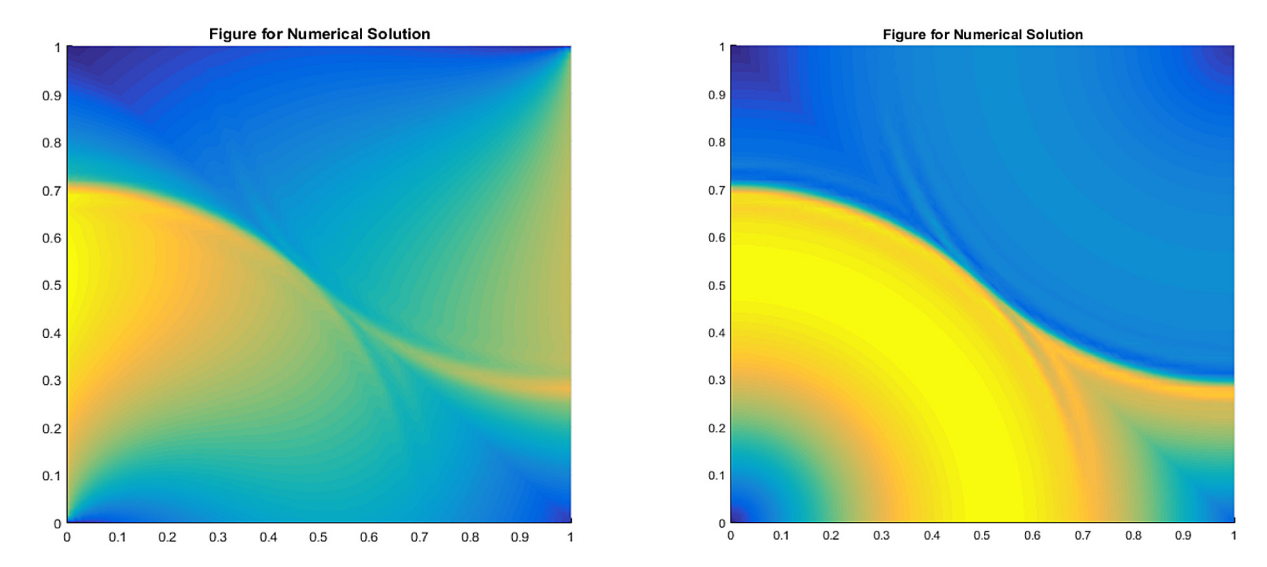


Fig. 6.2. Contour plots of numerical solution λ_0 on the unit square domain Ω_1 ; $C^{-1} - P_2(T)/P_2(\partial T)/P_1(T)$ element; uniform triangular partitions; convection $\boldsymbol{\beta} = [-y, x]$ for y < 1 - x and $\boldsymbol{\beta} = [1 - y, x - 1]$ otherwise; reaction c = 0; the inflow boundary data $g = \sin(3x)\cos(5y)$; and $(\tau_1, \tau_2) = (1, 1)$. The load function f = 1 (left) and f = 0 (right).

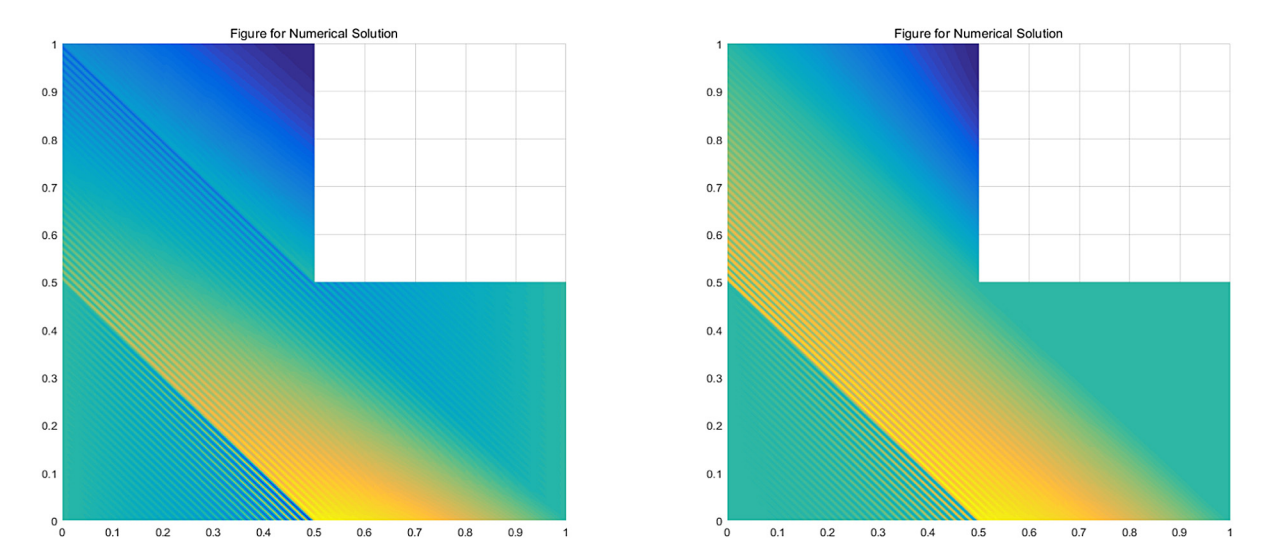


Fig. 6.3. Contour plots of numerical solution λ_0 on the L-shaped domain Ω_2 ; $C^{-1} - P_2(T)/P_2(\partial T)/P_1(T)$ element; uniform triangular partitions; convection $\boldsymbol{\beta} = [-1, 1]$ for y < 0.5 - x and $\boldsymbol{\beta} = [1, -1]$ elsewhere; reaction c = 1; the inflow boundary data $g = \sin(\pi x)\cos(\pi y)$; and $(\tau_1, \tau_2) = (1, 1)$. f = 1 (left) and f = 0 (right).

Fig. 6.4 is for the numerical solution λ_0 on the cracked unit square domain Ω_3 . The convection vector is given by $\beta = [0.5 - y, x - 0.5]$, the reaction is c = x - y, the inflow boundary data is $g = \sin(x)$, and $(\tau_1, \tau_2) = (1, 1)$. Fig. 6.4 in the left is for the load function f = 1, and the one on right is for f = 0.

Table 6.9 illustrates the computational performance of the algorithm on the cracked domain Ω_4 when the $C^{-1} - P_2(T)/P_2(\partial T)/P_1(T)$ element is used. The exact solution is $\lambda = \sin(\pi x)\sin(\pi y)$, the convection is $\beta = [2 - y, x]$, and the reaction is c = -1. The numerical results show that the convergence for ϵ_0 and ϵ_b in the L^2 norm are of the optimal order $\mathcal{O}(h^3)$ (see Fig. 6.5).

In summary, the numerical results from the primal–dual weak Galerkin finite element scheme (2.6)–(2.7) for the transport problem (1.1) confirm the theory developed in this paper. The numerical experiments reveal optimal-order of convergence for all the test cases. We are confident that the PDWG scheme is a stable, accurate, and convergent numerical method for the first-order transport problem in non-divergence form.

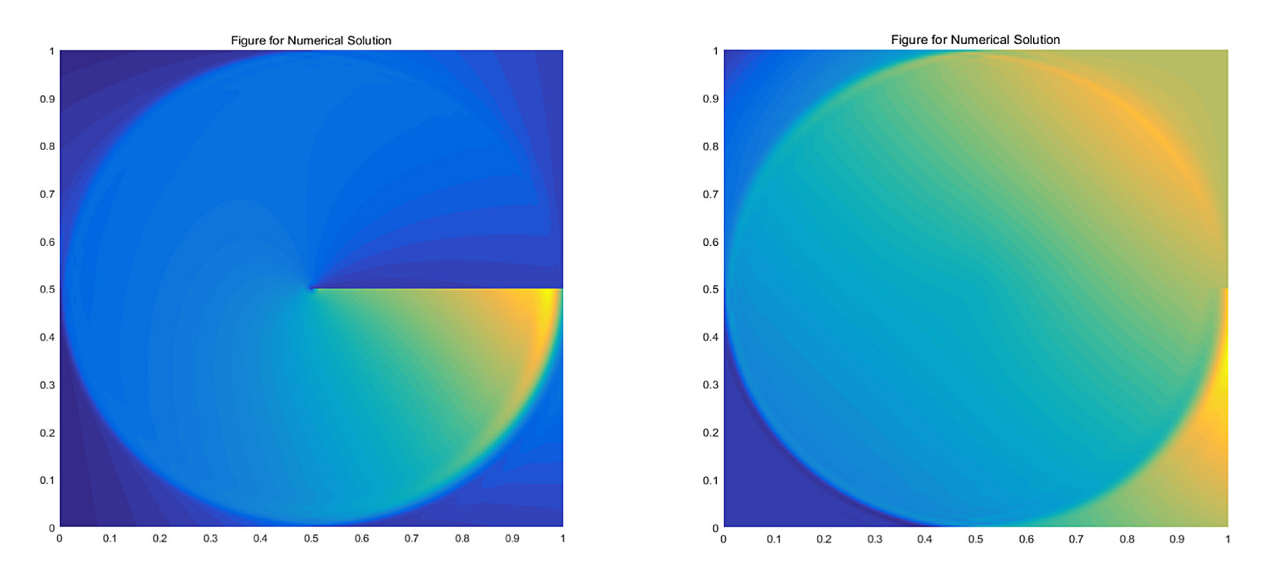


Fig. 6.4. Contour plots of numerical solution λ_0 on the cracked square domain Ω_3 ; $C^{-1} - P_2(T)/P_2(\partial T)/P_1(T)$ element; uniform triangular partitions; convection $\boldsymbol{\beta} = [0.5 - y, x - 0.5]$; reaction c = x - y; the inflow boundary data $g = \sin(x)$; and $(\tau_1, \tau_2) = (1, 1)$. f = 1 (left) and f = 0 (right).

Table 6.9 Numerical rates of convergence for the $C^{-1} - P_2(T)/P_2(\partial T)/P_1(T)$ element with the exact solution $\lambda = \sin(\pi x)\sin(\pi y)$ on the cracked domain Ω_4 ; uniform triangular partitions; convection vector $\boldsymbol{\beta} = [2-y,x]$; reaction coefficient c=-1; and the parameters $(\tau_1,\tau_2)=(0,1)$.

	1/h	$\ \epsilon_0\ $	Order	$\ \epsilon_b\ $	Order	$\ e_h\ $	Order
	4	1.8937E-02	2.9572	3.3943E-02	3.0853	8.8951E-02	1.4150
	8	2.2397E-03	3.0798	4.0766E-03	3.0577	2.3357E-02	1.9291
	16	2.4510E-04	3.1919	4.5456E-04	3.1648	5.5016E-03	2.0860
	32	2.7712E-05	3.1448	5.2391E-05	3.1171	1.2981E-03	2.0834

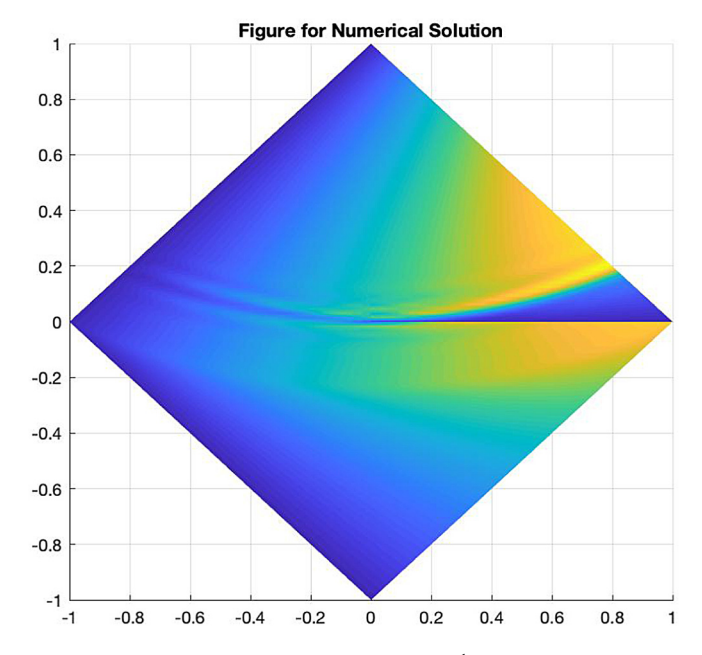


Fig. 6.5. Plots of numerical solution λ_0 on the cracked square domain Ω_4 using the $C^{-1} - P_2(T)/P_2(\partial T)/P_1(T)$ element; uniform triangular partitions; convection $\boldsymbol{\beta} = [2 - y, x]$; reaction c = y - x; inflow boundary data g = 0; load function f = 1 and $(\tau_1, \tau_2) = (1, 1)$.

References

- [1] C. Wang, J. Wang, A primal-dual weak Galerkin finite element method for second order elliptic equations in non-divergence form, Math. Comput. 87 (2018) 515-545.
- [2] C. Wang, J. Wang, A primal-dual finite element method for first-order transport problems, J. Comput. Phys. 417 (2020) 109571.
- [3] C. Wang, J. Wang, A primal-dual weak Galerkin finite element method for Fokker-Planck type equations, SIAM Num. Anal. 58 (5) (2020) 2632-2661.
- [4] C. Wang, J. Wang, Primal-dual weak Galerkin finite element methods for elliptic Cauchy problems, Comput. Math. Appl. 79 (3) (2020) 746-763.
- [5] C. Wang, L. Zikatanov, Low regularity primal-dual weak Galerkin finite element methods for convection-diffusion equations, J. Comput. Appl. Math. 394 (2021) 113543.
- [6] C. Wang, A new primal-dual weak Galerkin finite element method for Ill-posed elliptic Cauchy problems, J. Comput. Appl. Math. 371 (2020) 112629.
- [7] W. Cao, C. Wang, New primal-dual weak Galerkin finite element methods for convection-diffusion problems, Appl. Numer. Math. 162 (2021) 171–191.
- [8] D. Li, C. Wang, A simplified primal-dual weak Galerkin finite element method for Fokker-Planck type equations, arXiv:2004.13817.
- [9] S. Cao, C. Wang, J. Wang, A new numerical method for div-curl systems with low regularity assumptions, arXiv:2101.03466.
- [10] W. Cao, C. Wang, J. Wang, A new primal-dual weak galerkin method for elliptic interface problems with low regularity assumptions, arXiv:2010.14564
- [11] C. Wang, Low regularity primal-dual weak galerkin finite element methods for Ill-posed elliptic cauchy problems, arXiv:2011.12377.
- [12] W. Cao, C. Wang, J. Wang, An L^p-primal-dual weak galerkin method for convection-diffusion equations, arXiv:2111.11005.
- [13] C. Wang, A modified primal-dual weak Galerkin finite element method for second order elliptic equations in non-divergence form, Int. J. Numer. Anal. Model. 18 (2021) 500–523.
- [14] E. Burman, Stabilized finite element methods for nonsymmetric, noncoercive, and ill-posed problems. Part I: Elliptic equations, SIAM J. Sci. Comput. 35 (6) (2013) A2752–A2780.
- [15] E. Burman, Stabilized finite element methods for nonsymmetric, noncoercive, and ill-possed problems. Part II: hyperbolic equations, SIAM J. Sci. Comput. 36 (4) (2014) A1911–A1936.
- [16] J. Wang, X. Ye, A weak Galerkin mixed finite element method for second-order elliptic problems, Math. Comp. 83 (2014) 2101-2126.